ADHESIVE STRESSES IN AXIALLY-LOADED TUBULAR BONDED JOINTS - PART I: CRITICAL REVIEW AND FINITE ELEMENT ASSESSMENT OF PUBLISHED MODELS

E. Dragoni[a], L. Goglio[b*]

[a]Department of Engineering Sciences and Methods, Università di Modena e Reggio Emilia, via Amendola 2, 42100 Reggio Emilia, Italy

[b]Department of Mechanical and Aerospace Engineering, Politecnico di Torino, corso Duca degli Abruzzi 24, 10129 Torino, Italy

Abstract

Adhesive bonding of overlapping coaxial tubes of either conventional or composite materials is a joining solution often encountered in engineering structures. This paper reviews the underlying assumptions and assesses the accuracy of five published theoretical models for the adhesive stresses produced by axial loading of the tubular joint. The models scrutinized are those by Lubkin and Reissner (1956), Shi and Cheng (1993), Nayeb-Hashemi et al. (1997), Pugno and Carpinteri (2003) and Nemeş et al. (2006). Comparison of the model results with the outcome of ad-hoc finite element analyses on five joint configurations shows that: 1) all models predict correctly the shear stresses; 2) only Lubkin and Reissner's model gives correct peel stress distributions; 3) the axial and the hoop stresses are close to each other and are about one half of the peel stresses. The usefulness of an explicit closed-form solution, not provided by Lubkin and Reissner's theory, is recognized.

[*]Corresponding author. Tel. +39 011 0906934; Fax: +39 011 0906999; E-mail: luca.goglio@polito.it

Keywords: C: Stress distribution; C: Finite element stress analysis; E: Joint design; Cylindrical joint.

Nomenclature

Notations in Lubkin and Reissner model [1] and FE analysis

a, a_1, a_2	Mean radii of adhesive layer, tube 1 and tube 2
A_{ij} , C_i	Known coefficients in the differential equation set
c	Half of overlap length
D_1, D_2	Bending stiffnesses of tubes 1 and 2
E	Young's modulus of both tubes in the case study joints
E_1, E_2	Young's moduli of tube 1 and tube 2
E_a , G_a	Young's and shear moduli of adhesive
g_1, g_2, g_3	Dimensionless functions
F	Axial load applied to the joint
M_1, M_2	Longitudinal bending moments acting on tubes 1 and 2 at position x
N_1, N_2	Hoop forces acting on tubes 1 and 2 at position x
s	Complex Laplacian variable
t	Thickness of both tubes in the case study joints
t_1, t_2	Thicknesses of tubes 1 and 2
T_1, T_2	Axial forces acting on tubes 1 and 2 at position x
u_1, u_2	Axial displacements of tubes 1 and 2

V_1, V_2	Shear forces acting on tubes 1 and 2 at position x
w_1, w_2	Radial displacements of tubes 1 and 2
x, y, z	Axial, radial and hoop axes of the reference coordinate system
β	"Elastothickness" parameter (= $\eta E/tE_a$)
η	Thickness of adhesive layer
$d\theta$	Infinitesimal circumferential angle
ν_1, ν_2	Poisson's ratios of tubes 1 and 2
σ, τ	Generic peel and shear stresses
σ_x	Axial stress evaluated at mid-thickness of the adhesive layer
$\sigma_{x\,max}$	Max value of σ_x
σ_y	Peel stress evaluated at mid-thickness of the adhesive layer
$\sigma_{y\,max}$	Max value of σ_y
σ_z	Hoop stress evaluated at mid-thickness of the adhesive layer
$\sigma_{z\,max}$	Max value of σ_z
τ_m	Mean shear stress acting at mid-thickness of the adhesive layer
τ_{xy}	Shear stress evaluated at mid-thickness of the adhesive layer
$\tau_{xy\,max}$	Max value of τ_{xy}

1. Introduction

Coaxial circular tubes can be effectively joined by adhesive bonding, since this geometrical configuration provides wide area in limited space and the adhesive is loaded mainly (or exclusively, in case of pure torsion) by shear stresses. The use of this geometry in practical applications is widespread, especially to join multimaterial or composite tubings for lightweight structures. Surprisingly, this joint type has been investigated in the technical literature considerably less than those involving flat geometries, i.e. single or double lap joints.

Focusing the attention on the condition of axial loading, the starting point is the pioneering work by Lubkin and Reissner [1], who treated the tubular joint under the same main assumptions as used for the flat lap joints [2]. In Lubkin and Reissner's model, the adherends are subjected to tension, shear and bending, while the adhesive transmits shear and peel stresses (the remaining components being disregarded) that are a function of the axial coordinate only. Subsequent models in the literature [3-9] have adopted different approaches. Several models reduce the complexity of the problem by assuming that the adherends are subjected to tension only [4-9]. Conversely, a more complex stress state in the adhesive is assumed, admitting the through-thickness variation of the stresses [3,4,6-9] and/or the existence of other stress components [3,5-9].

The aim of the present work is to critically review the literature concerned with this problem, compare the results produced by the different models and point out the inadequacies. Finite element (FE) results on a range of joint configurations are used as numerical benchmark, extending the analyses presented in [10]. The need for an analytical, closed-form solution is also highlighted, and the related difficulties, not

explicitly overcome [1], are discussed.

2. Review of theoretical models

As reminded in the Introduction, the axisymmetric lap bonded joint has received much less attention in the technical literature, compared to the cases of the flat single- and double-lap joints. Within this work, the following studies and the corresponding analytical models have been found and considered:

- Lubkin and Reissner (1956) [1];
- Shi and Cheng (1993) [3];
- Nayeb-Hashemi, Rossettos and Melo (1997) [4];
- Pugno and Carpinteri (2003) [5];
- Nemeş, Lachaud and Mojtabi (2006) [6], Nemeş and Lachaud (2009) [7].

For each of these models a brief description is given separately in this section, accounting for the starting assumptions and the solutions obtained. Other studies, related to the problem of the tubular joint but not presenting analytical models, are mentioned as well.

2.1. Lubkin and Reissner model

The study presented by Lubkin and Reissner [1] extends, to the axisymmetric case, the typical approach used for the flat single lap joint [2] with the following assumptions:

- The adherends (tubes) are thin shells subjected to axial tension force, shear force and bending moment; therefore, in particular, the axial stress is not constant over the thickness;

- The adhesive is an elastic medium, in practice a spring layer, transmitting shear (longitudinal) and peel (radial) stresses. Both stresses are constant over the adhesive thickness and are a function of the axial coordinate only. Circumferential shear stresses are not considered because they would imply torsion of the joint;
- The kinematics of the tubes is expressed in terms of axial displacement (due to tension and bending), radial displacement and rotation (due to bending);
- Due to the axisymmetric geometry the rotation of the overlap is small, thus the need to account for it, which leads to the "moment factor" in the case of the flat joint [2], does not arise (this aspect will be reconsidered below in light of FE results and theoretical considerations).

Therefore, such assumptions are consistent with those of the models proposed for the flat joints, the only extension being the use of axisymmetric conditions instead of plane strain. Unfortunately, such extension implies a more complicated mathematical coupling of the variables, compared to the case of flat joints; thus it is no longer possible to obtain separate differential equations for the shear and peel stresses (as done, for instance, in [11]).

Another important consequence of the assumptions is that also the regions of the tubes near the overlap are subjected to bending and shear, which progressively vanish moving from the overlap end, like the case of a cylindrical vessel in the region near the end [12]. The implication is that the boundary conditions at the ends of the overlap are not of simple axial loading (which is true for the tubes at sufficient distance from the joint) and must be found by imposing continuity of force, moment, displacement and rotation at the transition section between the overlapping and non-overlapping parts of

each tube.

The analytical treatment is outlined in brief in the Appendix of the original work [1]; considering the free body diagrams of Fig. 1, the equilibrium equations are the following (the plus or minus sign is associated with the tube index i = 1,2 respectively):

$$a_i \frac{dT_i}{dx} \pm a\tau = 0 \tag{1}$$

$$a_i \frac{dV_i}{dx} - N_i \pm a\sigma = 0 \tag{2}$$

$$a_i \frac{dM_i}{dx} - a_i V_i + a\frac{t_i}{2}\tau = 0 \tag{3}$$

where T_i, N_i, M_i are, respectively, the axial force per unit length, the hoop force per unit length and the bending moment per unit length in the i-th tube; a and a_i are the mean radii of the adhesive layer and of the i-th tube. The related elasticity equations are written in the form:

$$\frac{d^2 w_i}{dx^2} = -\frac{M_i}{D_i} \tag{4}$$

$$\frac{du_i}{dx} = \frac{T_i - \nu_i N_i}{E_i t_i} \tag{5}$$

$$\frac{w_i}{a_i} = \frac{N_i - \nu_i T_i}{E_i t_i} \tag{6}$$

where $D_i = E_i t_i^3 / 12(1-\nu_i^2)$ is the bending stiffness.

The list of equations is completed by the adhesive stress-strain relationships:

$$\sigma = \frac{E_a}{\eta}(w_2 - w_1) \tag{7}$$

$$\tau = \frac{G_a}{\eta}\left[\left(u_2 + \frac{t_2}{2}\frac{dw_2}{dx}\right) - \left(u_1 - \frac{t_1}{2}\frac{dw_1}{dx}\right)\right] \tag{8}$$

The analytical treatment leads to a set of three differential equations, two of the fourth order and one of the second order, in the three dimensionless functions g_1, g_2, g_3 (which correspond, respectively, to the normalized displacements w_1, w_2 and to the

difference of axial forces in the tubes). Although the authors conclude that the solution is possible by standard methods, they report no explicit form of it. Instead, a table collecting the results in terms of normalized shear and peel stresses is given for a set of 48 cases, under varying values of input data (this aspect will be reconsidered in detail in a section 4.2). It is noticed that the stress field is qualitatively similar to the case of flat single lap joint: the stress distribution is relatively flat in the central part of the overlap and peaks at the ends; it is more uniform in case of short overlap and/or "soft" adhesive. In all models of the joints defined in this way, no attempt is made to account for the stress singularity at the end corners; the stress distribution obtained can be regarded as representative of the situation at mid-thickness of the adhesive.

2.2. Shi and Cheng model

This work [3] approaches the case of the tubular joint in a wider perspective than [1], to include also cases of thick tubes. The main starting assumptions of this model are (stress components expressed in the reference frame $r\theta z$, which are respectively the radial, hoop and axial coordinates):

- All axisymmetric stress components, namely σ_r (normal, radial), σ_θ (normal, hoop), σ_z (normal, axial) and τ_{rz} (shear, radial-axial) are present in the adherends;
- The stress σ_z in the adhesive is negligible.

Since the loading state of the tubes is not described by in-plane (membrane) forces and bending moments (typical of shells), the solution is sought directly in terms of stresses. For each part, the radial and axial equilibrium equations are written as:

$$\frac{\partial \sigma_r}{\partial r} + \frac{\sigma_r - \sigma_\theta}{r} + \frac{\partial \tau_{rz}}{\partial z} = 0 \tag{9}$$

$$\frac{\partial \sigma_z}{\partial z} + \frac{\partial \tau_{zr}}{\partial r} + \frac{\tau_{zr}}{r} = 0 \tag{10}$$

The compatibility equations are expressed in terms of stresses as:

$$(1+\nu)\frac{\sigma_r - \sigma_\theta}{r} - \frac{\partial}{\partial r}\left[\sigma_\theta - \nu(\sigma_r + \sigma_z)\right] = 0 \tag{11}$$

$$\frac{\partial}{\partial r}\left[\sigma_z - \nu(\sigma_r + \sigma_\theta)\right] + r\frac{\partial^2}{\partial z^2}\left[\sigma_\theta - \nu(\sigma_r + \sigma_z)\right] = 2(1+\nu)\frac{\partial \tau_{zr}}{\partial z} \tag{12}$$

Regarding the boundary conditions of the stresses, apart from the obvious continuity at the interfaces and zeroing at the unloaded surfaces, it is assumed that at the loaded ends of the overlap the axial stresses applied for continuity by the tubes out of the overlap are respectively f_1 in the inner tube and f_2 in the outer tube, given by the following equations:

$$f_1(r) = p_1 + p_3 r \tag{13}$$

$$f_2(r) = p_3 + p_4 r \tag{14}$$

where p_1, p_2, p_3, p_4 are constants. This assumption accounts for bending in the tubes.

The axial stresses σ_{z1} in the inner tube and σ_{z2} in the outer tube are as follows:

$$\sigma_{z1} = \phi_1(z) + r\,\phi_2(z) \tag{15}$$

$$\sigma_{z2} = \psi_1(z) + r\,\psi_2(z) \tag{16}$$

where $\phi_1(z)$, $\phi_2(z)$, $\psi_1(z)$, $\psi_2(z)$ are unknown functions of z to be determined. By means of long mathematical manipulations, the authors show that it is possible to express all joint stresses, in the adherends and in the adhesive, in terms of the two functions $\phi_1(z)$, $\phi_2(z)$ only. These functions are determined by minimization of the complementary energy (as defined in [13], pp. 29-31), which leads to the set of two differential equations

$$\frac{\partial F}{\partial \phi_1} - \frac{d}{\partial z}\frac{\partial F}{\partial \phi_1'} + \frac{d^2}{\partial z^2}\frac{\partial F}{\partial \phi_1''} = 0 \tag{17}$$

$$\frac{\partial F}{\partial \phi_2} - \frac{d}{\partial z}\frac{\partial F}{\partial \phi_2'} + \frac{d^2}{\partial z^2}\frac{\partial F}{\partial \phi_2''} = 0 \tag{18}$$

where the primes indicate differentiation with respect to z and F is a known function of $\phi_1(z)$, $\phi_2(z)$ and their first and second derivatives. The solution of the differential equations, linear with constant coefficients, leads to a characteristic equation which has eight solutions (i.e. eigenvalues).

Although the authors remark that their method yields closed-form solutions, these are not reported explicitly. Numerical results are given for two examples corresponding to cases of joints involving thin and thick tubes respectively.

2.3. Nayeb-Hashemi, Rossettos and Melo model

In this work concerned with the behaviour of tubular joints under tension/torsion fatigue [4], the authors search for a solution for the stress due to axial loading (the case of torsional loading, developed as well in [4], is out of scope of the present paper), based on a shear lag model (Fig. 2). The starting assumptions in this case are:

- The adherends are subjected only to tension, causing constant axial stress over the thickness;
- The adhesive is an elastic medium, only transmitting shear stress, which is a function of the axial and radial positions (i.e. it is not constant over the thickness).

In addition, the authors deal with the case of incomplete bonding, by assuming that an annular region is not connected by the adhesive. This case is out of our scope and will not be considered here. Considering an infinitesimal length of joint, the equations for axial equilibrium expressed in terms of axial displacements are, respectively for tube 2 and 1:

$$E_2\pi\left(R_4^2 - R_3^2\right)\frac{d^2u_2}{dx^2} - 2\pi R_3\tau_{rx2} = 0 \tag{19}$$

$$E_1\pi\left(R_2^2 - R_1^2\right)\frac{d^2u_1}{dx^2} + 2\pi R_2\tau_{rx1} = 0 \tag{20}$$

where R_1, R_2, R_3, R_4, are the inner and outer radii of the tubes (see also Fig. 2), u_1 and u_2 the axial displacements, E_1 and E_2 the elastic moduli, τ_{rx1} and τ_{rx2} the tangential stresses at the interfaces with the adhesive (note that in the original article the term $2\pi R_2\tau_{rx1}$ in (20) is mistakenly written with a "–" sign, which propagates through the mathematical derivations). The axial equilibrium of an infinitesimal annular element of adhesive reads

$$\tau_a dr + r\, d\tau_a = 0 \tag{21}$$

Relating the shear stress in the adhesive to the displacements by means of the elastic modulus G_a, two simultaneous differential equations in u_1 and u_2 are found from (19) and (20); the related solutions are written as:

$$u_1(\xi) = \frac{1}{E_1\left(R_2^2 - R_1^2\right)}\left[C_1\xi + C_2 - E_2\left(R_4^2 - R_3^2\right)u_2\right] \tag{22}$$

$$u_2(\xi) = C_3 e^{\theta_a\xi} + C_4 e^{-\theta_a\xi} - \frac{1}{\theta_a^2}B\left(C_1\xi + C_2\right) \tag{23}$$

where $\xi = x/L$ is the dimensionless abscissa, $C_1 - C_4$ are the integration constants obtained from the known loading conditions at the ends of each tube (respectively P or zero, see Fig. 2), θ_a is the solution of the eigenequation given by

$$\theta_a = \sqrt{\frac{2G_a}{\ln R_3 - \ln R_2}\left[1 + \frac{E_2\left(R_4^2 - R_2^2\right)}{E_1\left(R_2^2 - R_1^2\right)}\right]\frac{L^2}{E_2\left(R_4^2 - R_2^2\right)}} \tag{24}$$

and B is a constant defined as

$$B = -\frac{2G_a L^2}{\left(\ln R_3 - \ln R_2\right)E_1E_2\left(R_4^2 - R_3^2\right)\left(R_2^2 - R_1^2\right)} \tag{25}$$

Once the displacements u_1, u_2 are known, the stress in the adhesive is calculated as:

$$\tau_a = \frac{G_a}{\ln R_3 - \ln R_2} \frac{u_2 - u_1}{r} \tag{26}$$

Thus, the stress distribution given by equation (26) is:

- In the axial direction, a direct consequence of the exponential and linear variations along the overlap of the displacements (22), (23);
- In the radial direction, inversely proportional to the local radius.

2.4. Pugno and Carpinteri model

The work by Pugno and Carpinteri [5] proposes a solution for the tubular joint, again based on a shear lag model, which is then applied to the optimization of the joint geometry (variation of the tube cross section), to the analysis of crack propagation and to crack detection by vibration frequency measurement. The related starting assumptions are:

- The adherends are subjected only to tension, causing constant axial stress over their thickness;
- The adhesive is a thin elastic medium, therefore the stress state is considered constant over its thickness; the predominant term is the shear stress, but also the other stress components are considered.

Also in this model (Fig. 3) the study starts from the axial equilibrium, considering tube 1:

$$\tau_{rx} = -\frac{1}{2\pi R} \frac{dN_1}{dx} \tag{27}$$

where N_1 is the axial force in the tube (note that, to avoid possible confusion with the model in [1], here the symbol N is used to designate the axial force in the tubes). The shear stress in the adhesive is related to the shear strain by

$$\tau_{rx} = G_a \gamma_{rx} \tag{28}$$

Considering the elasticity of the tubes, their axial elastic displacements u_1, u_2 are written as

$$u_1 = \int \frac{N_1}{E_1 A_1} dx \tag{29}$$

$$u_2 = \int \frac{N_2}{E_2 A_2} dx \tag{30}$$

where N_i, E_i, A_i, are, respectively, axial force, Young's modulus, cross section of the tube i=1,2. Thus, the shear strain can be related to the tube displacements by

$$u_2 - u_1 = h\,\gamma_{rx} \tag{31}$$

Introducing the auxiliary function $f(x)$, such that $N_1 = N\,f(x)$ and $N_2 = N\,(1 - f(x))$, a differential equation is written, the solution of which is

$$f(x) = C_1 \mathrm{e}^{\alpha x} + C_2 \mathrm{e}^{-\alpha x} + \beta \tag{32}$$

where the integration constants C_1, C_2 are obtained from the loading at the ends of the joint (axial force either N or zero, see Fig. 3), and α is given by the eigensolution

$$\alpha = \sqrt{\frac{2\pi R G_a}{h} \frac{\left(E_1 A_1 + E_2 A_2\right)}{E_1 A_1 E_2 A_2}} \tag{33}$$

and the constant β is

$$\beta = \frac{E_1 A_1}{E_1 A_1 + E_2 A_2} \tag{34}$$

Then, the adhesive shear stress is obtained by the equilibrium equation (27). In addition, the remaining stress components are obtained by assuming that the adhesive is subjected to the strains imposed by the adherends. Denoting v_i (i =1, 2) the radial displacements of the tubes (produced by the axial stress because of Poisson's effect), the radial (ε_r), hoop (ε_θ) and axial (ε_x) strains in the adhesive are, respectively:

$$\varepsilon_r = \frac{v_1 - v_2}{h} \tag{35}$$

$$\varepsilon_\theta = \frac{1}{2}\frac{v_1 + v_2}{R} \tag{36}$$

$$\varepsilon_x = \frac{1}{2}\frac{d(u_1 + u_2)}{dx} \tag{37}$$

Thus, the corresponding radial (σ_r), hoop (σ_θ) and axial (σ_x) stresses in the adhesive are obtained by using standard three-dimensional elasticity equations.

2.5. Nemeş, Lachaud and Mojtabi; Nemeş and Lachaud models

These two works [6,7] assume a more complicated stress state in the parts (tubes and adhesive layer) of the joint, as well as non-isotropic elastic behaviour of the tubes. The basic assumptions are:

- the adherends are subjected to axial stress (originated by the tension) constant over the thickness, as well as to shear (longitudinal-radial) and hoop stresses, both variable over the thickness;
- the adhesive is subjected to shear and hoop stresses, both variable over the thickness.

In [6], the analytical treatment starts from the general equilibrium equations in cylindrical co-ordinates, which in radial (r) and axial (z) directions read respectively:

$$\frac{\partial \tau_{rz}}{\partial z} - \frac{1}{r}\sigma_{\theta\theta} = 0 \tag{38}$$

$$\frac{\partial \sigma_{zz}}{\partial z} + \frac{\partial \tau_{rz}}{\partial r} + \frac{1}{r}\tau_{rz} = 0 \tag{39}$$

Hence for the inner tube (superscript 1), the adhesive (superscript c) and the outer tube (superscript 2) the related equilibrium equations are written (see Fig. 4 for dimensions and axes).

Inner tube (1). The equilibrium of an infinitesimal length gives

$$\tau_{rz}^{(1)} = \frac{r_i^2 - r^2}{2r}\frac{d\sigma_{zz}^{(1)}}{dz} = 0 \tag{40}$$

Replacing the latter result in eq. (38), also the hoop stress can be related to the axial stress:

$$\sigma_{\theta\theta}^{(1)} = \frac{r_i^2 - r^2}{2}\frac{d^2\sigma_{zz}^{(1)}}{dz^2} = 0 \tag{41}$$

Adhesive (c). Considering eq. (39) and assuming continuity of shear stress at the interface between inner tube and adhesive, a relationship between shear stress in the adhesive and axial stress in the inner tube is obtained:

$$\tau_{rz}^{(c)} = \frac{r_i^2 - r_{ic}^2}{2r}\frac{d\sigma_{zz}^{(1)}}{dz} = 0 \tag{42}$$

In the same way as for the inner tube, also an expression for the hoop stress in the adhesive is found:

$$\sigma_{\theta\theta}^{(c)} = \frac{r_i^2 - r_{ic}^2}{2}\frac{d^2\sigma_{zz}^{(1)}}{dz^2} = 0 \tag{43}$$

Outer tube (2). Considering twice the axial equilibrium of an infinitesimal length of joint (in one case taking the whole cross section and in the other case taking only the zone exceeding the generic radius *r* in the outer tube) gives

$$\tau_{rz}^{(2)} = \frac{\left(r_e^2 - r^2\right)\left(r_{ic}^2 - r_i^2\right)}{2r\left(r_{ec}^2 - r_e^2\right)}\frac{d\sigma_{zz}^{(1)}}{dz} = 0 \tag{44}$$

Applying once again eq. (38) the hoop stress can be related to the axial stress in the inner tube:

$$\sigma_{\theta\theta}^{(2)} = \frac{\left(r_e^2 - r^2\right)\left(r_{ic}^2 - r_i^2\right)}{2\left(r_{ec}^2 - r_e^2\right)}\frac{d^2\sigma_{zz}^{(1)}}{dz^2} = 0 \tag{45}$$

After all stresses have been expressed as a function of the axial stress in the inner tube, the potential energy is written and, by minimization, the following final differential equation is obtained

$$E\frac{d^4\sigma_{zz}^{(1)}}{dz^4}+(B-C)\frac{d^2\sigma_{zz}^{(1)}}{dz^2}+A\sigma_{zz}^{(1)}+\frac{D}{2}=0 \tag{46}$$

in which *A*, *B*, *C*, *D* and *E* are constants.

In the rest of the paper [6] no further analytical detail is given, the authors show graphically the results in terms of distributions of the various stresses, studying the influence of overlap length, thickness and elastic modulus of the adhesive, and ratio of the elastic moduli of the tubes.

This model is refined by Nemeş and Lachaud in [7], by including in the joint also the radial stress, which is assumed to be constant in the adhesive and a function of the radial coordinate alone in the tubes. The authors notice that adding this component has also a significant influence on the distributions of the shear (longitudinal) and circumferential stresses; in their results the circumferential component is the highest.

An analytical treatment developed on the same basis as the model in [6] has been used by Kumar [8] and Kumar and Scanlan [9] to study two cases of functionally graded adhesive modulus, with different formulations. The model in [6] has also been applied by Martinez et al. [14] to evaluate the shear stresses in a pin-and-collar specimen.

3. Case studies

3.1. Test configurations

With reference to the general configuration in Fig. 5, Table 1 lists the dimensions, the elastic properties and the axial load of the five joints used as case studies. These configurations are taken from the set of 48 joints for which Lubkin and Reissner [1] provide numerical results (note that the symbols used in Table 1 and in the following presentation of the results are those adopted in [1]). As assumed by [1], the tubular

joints in Table 1 relate to the condition of "symmetric" adherends, i.e. adherends with the same thickness ($t_1 = t_2 = t$) and the same elastic properties ($E_1 = E_2 = E$, $\nu_1 = \nu_2 = \nu$). Apart from this simplification, necessary for the comparison of results, the configurations in Table 1 were chosen to explore the widest range of configurations offered by [1] in terms of geometry and material properties. In particular, Table 1 covers all the values investigated in [1] – namely 4, 20, 100 – for the "elastothickness" parameter $\beta = \eta E/tE_a$, which is a measure of the relative stiffness of adherends and adhesive. Parameter β cannot be too small, otherwise the underlying assumption of Lubkin and Reissner's model (comparatively flexible adhesive layer) is violated.

The axial forces F in Table 1 were defined so as to produce a unit mean shear stress ($\tau_m = F/4\pi a\, c = 1$ MPa) at mid-thickness of the adhesive. This choice allowed straightforward normalization of the stress results with respect to the mean shear stress. The joints in Table 1 were also analyzed under axial forces corresponding to a mean shear stress of 50 MPa. These analyses were performed to test the effect of geometric non-linearity (large deflections and rotations) on the stress response of the joint as described in Section 3.2.

3.2. FE modeling

Figure 6 shows the overall geometry with details of the FE mesh for the model of joint 1. Similar models were used also for the other joints in Table 1. The lengths of the tubes outside the overlap (*GC* and *DI* in Fig. 6) were 20 times the thickness t of each joint. According to the flexural theory for thin cylindrical shells [12], this condition ensured that the axial stress applied to the joints was perceived as a purely axial tension as assumed by the theoretical models in the literature. The FE models were

implemented with the Lusas software (LUSAS, Kingston upon Thames, UK), version 14.0.

Adherends and adhesive were discretized by 8-noded, quadratic axisymmetric solids with the elastic properties reported in Table 1. In all models, square elements were used for adherends and adhesives in the overlap region (*ABCD* in Fig. 6a,b). In this region the size of the squares was one-fourth of the adhesive thickness (0.25 mm). In the tube portions outside the overlap, the elements had a horizontal length increasing geometrically in the outward direction such that the outermost elements (close to lines *GH* and *IL* in Fig. 6a) were about six times the innermost ones. The optimal element size was identified with a mesh convergence procedure carried out on joint 1. Four models were analyzed with one, two, four and eight elements through the adhesive thickness (line *EF* in Fig. 6b,c) and keeping the square shape throughout the overlap. The stress results at mid-thickness (line *mn* in Fig. 6c), which are the natural counterpart for comparison of the stresses given by models such as Lubkin and Reissner's, changed negligibly on passing from two elements (Fig. 6) to eight elements. Consequently, the mesh density shown in Fig. 6 with four elements on line *EF* was retained as a trade-off between accuracy and efficiency.

The models were constrained by suppressing the axial degree of freedom of the nodes along the side *GH* in Fig. 6 and were loaded by applying a constant axial stress to the line *IL*. The value of the axial traction was defined so as to produce a total force on the tubes equal to the values shown in Table 1.

The models in Table 1, with the forces listed in the second last column, were analyzed within the linear elasticity framework. In particular, any non-linear effects arising from large deflections or rotations of the thin tube walls were neglected, exactly

as they are disregarded in the above-mentioned literature theoretical models. The results of these linear analyses were used for the comparison with the literature models. The joints loaded under a mean shear stress in the adhesive up to 50 MPa (see above) were analyzed by including geometrically non-linear effects with a total Lagrangian approach. These analyses were used only to see the real effect of geometric non-linearities on the stress results.

Figure 7 shows the distribution of axial stresses (σ_x) on the deformed configuration of joint 1 (linear analysis). The displacements are enlarged 500 times with respect to the actual values. Figure 8 displays the contour plot of the primary shear stresses (τ_{xy}) in the magnified region of the joint close to the left end of the overlap. The distributions of all available stresses (shear, τ_{xy}; peel, σ_y; hoop, σ_z; axial, σ_x; the subscripts refer to the coordinate system shown in Fig. 6a) are plotted in Fig. 9 for the five joints of Table 1. For the particular choice of the forces applied to the models (see Table 1), the stresses in Fig. 9 can be regarded as values normalized over the mean shear stress acting on the adhesive. These stresses were read along the mid-thickness (line *mn* in Fig. 6) of the adhesive layer. Table 2 displays the stress results as a function of the applied load for the geometrically non-linear analysis on Joint 1 (τ_m = 1, 10, 20, 30, 40, 50 MPa), together with the results from the linear model (τ_m = 1 MPa). Table 3 presents the ratios of non-linear to linear peak stresses in all joints under mean shear stresses of 1 and 50 MPa.

3.3. Theoretical results

For the same joint configurations considered in the FE modeling, in addition to the Lubkin and Reissner results, the stress state was calculated by means of the

analytical models by Nayeb-Hashemi *et al.* [4] and by Pugno and Carpinteri [5], for which the authors give a description detailed enough to allow for a (relatively) straightforward implementation. Using the model in [4], which accounts only for the shear stress including through-thickness variation, the values were calculated at mid-thickness of the adhesive. With the model in [5] all components – shear, peel, axial and hoop – were considered (in this case, constant over the thickness).

Figure 10 shows, in the same way as Fig. 9, the results for the five joints; the lines correspond to the various solutions (formulae), the isolated symbols are the values from the tables by Lubkin and Reissner. Regarding the latter, it must be pointed out that in the case of joint 2 – for which $2c/t = 2$, $R = 0.1$ and $\beta = 4$ according to Lubkin and Reissner – it has been noticed that the values published in [1] correspond in reality to $\beta = 5$. This finding has been made possible because the Lubkin and Reissner approach has been reconsidered and solved analytically with an alternative method, presented in detail in the part II of the present work [15].

4. Discussion

4.1. FE modeling

In the deformed shape shown in Fig. 7 it can be noticed that in the far ends of the non-overlapping zones of the tube the bending effects are small, because the profile of the wall remains straight and the axial stress is constant over the thickness. This argument confirms that the tube lengths adopted in the models outside the overlap are adequate. Obviously, the stress contour map in Fig. 8 evidences the elastic singularity in the corner *F*, well known in the literature (e.g. [16]), that can be limited by means of *ad hoc* local geometries as shown in [17] for the cylindrical assemblies. Apart from this,

the attention is focused here on the non-singular stresses in the mid-thickness line *mn* (Fig. 6), which in recent times have been reconsidered to formulate a criterion [18] which has given satisfactory results for preliminary joint design [19] (see Section 4.3).

Table 2 (non-linear analysis) shows that linear and non-linear stresses in Joint 1 are almost identical for a mean shear stress of 1 MPa and that the normalized non-linear stresses change only slightly as the load increases from the minimum to the maximum load level. The shear stress decreases by 2.6% as the mean load value changes from 1 to 50 MPa. All normal stresses increase, with a maximum variation of 7.7% for the peel component and slightly more than 5% for the other two.

Table 3 shows a similar pattern for all the joints examined, with the linear and non-linear stresses being nearly the same under a mean shear stress of 1 MPa. The effect of non-linearity on the stresses is generally contained within a few percent of the linear stresses up to the maximum applied stress (50 MPa). The only exception is represented by Joints 3 and 5 in which the non-linear normal stresses exceed the linear predictions by 20-30 percent under a mean shear stress of 50 MPa. However, since 50 MPa of mean average shear is a huge stress level, much higher than is sustainable by real adhesives, it can be concluded that the geometrically non-linear effects are negligible and, therefore, the linear analysis is adequate for this type of joint.

This latter aspect can be considered in a different perspective by comparison with the flat lap joint. Indeed, the case of a flat lap joint can be regarded as a limit condition achieved when the radii of the tubes become much larger than the thickness of the tubes, as it appears from the equations of Lubkin and Reissner [1] and from the numerical FE results of Hosseini and Oechsner [20]; the latter authors remark also that the cylindrical overlap approaches the behaviour of the TAST (Thick Adherend Shear Test) specimen,

with higher joint stiffness and stress uniformity than the single lap. Therefore, if for given thicknesses, moduli and overlap, the geometrical non-linearity is limited in the case of flat joint, *a fortiori* it becomes negligible in the case of cylindrical joint. A simple way to evaluate analytically the geometrical non-linearity for the flat lap joint is given by the moment factor *k* defined by Goland and Reissner [2], which accounts for the reduction in bending moment in the joint related to the self-alignment due to the joint rotation and is given by the expression

$$k = \frac{\cosh(u_2 c)}{\cosh(u_2 c) + 2\sqrt{2}\sinh(u_2 c)} \tag{47}$$

where: $u_2 = \sqrt{T/D_2}$, T is the tensile force per unit width, D_2 is the bending stiffness of the joint, c is the half overlap length. Applying equation (47) to the five cases, as reported in the bottom line of Table 3, it is found that in the case of 1 MPa mean shear stress *k* ranges between 0.90 and 0.98, thus close to unity. Therefore, it can be concluded that also from this viewpoint the geometrical non-linearity is negligible. In contrast, the *k* factor for a mean shear stress of 50 MPa implies a stress variation with respect to the linear assumption much higher than is found for cylindrical joints.

4.2. Comparison between FE and theoretical results

Considering the convergence analysis and the non-linear case mentioned above, the FE results cast no doubt on the adequacy of the mesh, thus the stresses at mid-thickness of the adhesive can be considered correct and used as a reference to validate those given by the theoretical models. Considering first the stress distributions in Fig. 9, in which the FE results are compared with the values given by Lubkin and Reissner [1], it appears that in general terms this analytical model reproduces reasonably well the

stress distribution, with the stress peaks at both overlap ends (the maximum of which is at the end of the outer tube). This is particularly true regarding the shear stresses, for all considered joints 1-5. Clearly, the solution by Lubkin and Reissner cannot fulfil the zero boundary conditions at the ends of the overlap; however, the peak values are correct. Conversely, some discrepancies affect the peak values of the peel stress that are in general slightly underestimated by the model, especially for joint 2, which is relatively thick-walled. This is a typical limitation of this kind of models (based on the assumption of thin plates or shells), evidenced for instance in [21] for the case of double lap joints. Indeed, the peel stresses given by the Lubkin and Reissner's solution fit better the FE results for joints 1 and 4, which are thin-walled; moreover, in the case of joint 2 the "elastothickness" parameter is small, and this is also unfavourable to the precision. The FE model gives also the values of the axial and hoop stresses; it is apparent that in all cases their values, although not negligible, are significantly lower (about one half) than the peel stress.

Extending the comparison to the models by Nayeb-Hashemi *et al*. [4] and by Pugno and Carpinteri [5], shown in Fig. 10, taking now the Lubkin and Reissner results as reference, a large difference in behaviour is noticed between the cases of shear and peel stresses. Indeed, the shear stress is described with higher precision by both models, which reproduce precisely the Lubkin and Reissner results and are indistinguishable from each other (the curves are exactly superimposed). Regarding the latter aspect, it can be remarked that, even if the analytical formulations [4] and [5] appear different, the behaviour of the tubes is described in the same way (simple tension, axial stress constant in the cross section); consequently, the shear lag is the same as well. Moreover, the variation of the shear stress in the adhesive thickness assumed by Nayeb-Hashemi *et*

al., proportional to 1/*r*, is in practice limited and the values at the interfaces of the adhesive with the inner or outer tubes are similar.

Considering now the peel stress, it is evident that the distribution given by the Pugno and Carpinteri model is, even qualitatively, completely different from that of Lubkin and Reissner and, as a consequence, also from FE. In Fig. 10, the values by Pugno and Carpinteri are positive at the left end of the distribution, i.e. the end of the outer tube, and negative at the right end, i.e. the end of the inner tube. The explanation for this fact can be found by observing that in the model in [5] the tubes are subjected to simple tension; therefore the radial displacements are due to shrinkage by Poisson's effect. At the left end, the outer tube is unloaded and does not shrink, the inner tube is loaded and shrinks, thus the radial gap between the tubes tends to increase and the peel stress is positive. At the right end, the inner tube is unloaded and does not shrink, whilst the outer tube is loaded and shrinks, thus the gap tends to decrease and the peel stress is negative. This kind of behaviour is contradicted by the present FE results, as well as by those shown by Adams and Peppiatt [10], which exhibit positive peel stress at both ends. The inadequacy of the model in [5] in predicting the peel stress is explained by the fact that bending in the tubes, which gives a significant effect on the radial displacement of the wall, is not included. Similarly, in the paper by Shi and Cheng [3] a peel stress distribution with opposite end signs is shown as well; this is surprising, since the axial stress corresponding to eqs. (15) and (16) should account for bending. To have a better insight on this fact, a FE analysis of the example 1 shown by these authors on page 594 and following of their work [3] was carried out. The obtained results are shown graphically in Fig. 11, this stress distribution is in accordance with the behaviour predicted by Lubkin and Reissner's model and the FE values of Adams and Peppiatt

[10], with positive peaks of peel stress at both overlap ends. Conversely, the peel stress distribution shown by Shi and Cheng in Figs. 3-5 of [3] changes monotonically along the overlap from positive (end of inner tube) to negative (end of outer tube) values, similar to the results given by [5] commented above. A possible explanation of this inadequacy could be that, although in [3] the bending behaviour is included, the transition from the overlap to the far ends of the tubes (included in Lubkin and Reissner's model as a harmonic, exponentially decaying deflection) is not considered by the Shi and Cheng's model.

The model by Pugno and Carpinteri [5] includes also the hoop and axial stresses in the adhesive, reported in Fig. 10 for the considered cases. Their values are always smaller (as absolute values) than the peel stress; however their distributions are similar to the peel stress profile, with opposite signs at the ends, in contrast with the FE findings in Fig. 9. An additional remark on the hoop stress is that in the model by Nemeş *et al*. [6] such component is even higher than the shear stress. This finding, confuted by all FE results, is a likely consequence of neglecting the peel stress, so that the hoop stress must increase to ensure equilibrium and compatibility. Nonetheless, also in the model in [7] the circumferential stress is the highest.

4.3. Relevance of the results and further work

With present FE software it is relatively easy to obtain the stress distribution in a cylindrical joint of this type. However, analytical modelling can still be useful because on the one hand a closed form solution implemented in a spreadsheet (or similar software tool) is faster in giving immediate answers when different design solutions must be tried (e.g. changing overlap, thickness, etc.), on the other hand it gives a better insight about the governing parameters than numerical results.

In the case of failure analysis of a joint, it would certainly be unavoidable to account for the adhesive behaviour including material non-linearity (plasticity, or even viscosity). Rational tools to this aim are fracture and/or damage mechanics (e.g. a cohesive model) to describe or predict separation of the substrates. Nonetheless, from the designer's viewpoint, a less sophisticated, but simpler and quicker, tool is useful in the preliminary design of the joint, and this can be obtained only by means of an elastic approach as adopted in this paper. In two previous papers [18,19] the authors have proposed a design criterion based on elastic, non-singular stresses, which was implemented in a computational tool [19] and applied to practical cases with a good degree of success. The present work is based on the same premises and is expected to give better results for more brittle than for more ductile adhesives. By pointing out the limitations of the literature models, the disclosed results provide a useful reference for first-approximation designs and to establish a correct starting point for further, more refined, theories. These arguments point out the need for an explicit, closed-form solution, which is presented in the second part of this work [15].

5. Conclusions

The classical case of a tubular bonded joint under axial load has been reconsidered and the stress solutions given by five literature models have been checked against expressly generated FE results for a range of joint configurations. The main conclusions are the following:

- The shear stress is in practice evaluated correctly by all models (apart from some discrepancies in the peak values, which is a general problem for the models based on plates);

- The peel stress is predicted correctly only by the Lubkin and Reissner [1] model, all the other models predict a negative peak at the end of the inner tube;
- The axial and hoop stress components are of similar order of magnitude and are about one half of the peel stress;
- The model by Lubkin and Reissner gives the best response and, therefore, deserves to be developed to achieve an explicit closed-form solution.

References

[1] J.L. Lubkin, E. Reissner. Stress distribution and design data for adhesive lap joints between circular tubes. Trans. ASME 1956;78:1213-1221.

[2] M. Goland, E. Reissner. The stresses in cemented joints. J. Appl. Mech.1944;11:A17-A27.

[3] Y.P. Shi, S. Cheng. Analysis of adhesive-bonded cylindrical lap joints subjected to axial load. J. Eng. Mech. 1993;119**:**584-602.

[4] H. Nayeb-Hashemi, J.N. Rossettos, A.P.Melo. Multiaxial fatigue life evaluation of tubular adhesively bonded joints. Int. J. Adhes. Adhes. 1997;17**:**55-63.

[5] N. Pugno, A. Carpinteri. Tubular adhesive joints under axial load. J. Appl. Mech. 2003;70**:**832-839.

[6] O. Nemeş, F. Lachaud, A. Mojtabi. Contribution to the study of cylindrical adhesive joining. Int. J. Adhes. Adhes. 2006;26:474-480.

[7] O. Nemeş, F. Lachaud. Modeling of cylindrical adhesively bonded joints. J. Adhesion Sci. Technol. 2009;23:1383-1393.

[8] S. Kumar. Analysis of tubular adhesive joints with a functionally modulus graded bondline subjected to axial loads. Int. J. Adhes. Adhes. 2009;29:785-795.

[9] S. Kumar, J.P. Scanlan. Stress analysis of shaft-tube bonded joints using a variational method. J. Adhesion 2010;86:369-394.

[10] R.D. Adams, N.A. Peppiatt. Stress analysis of adhesive bonded tubular lap joints, J. Adhesion 1977;9:1-18.

[11] D.A. Bigwood, A.D. Crocombe. Elastic analysis and engineering design formulae for bonded joints. Int. J. Adhes. Adhes. 1989;9**:**229-242.

[12] W.M. Coates. The state of stress in full heads of pressure vessels. Trans. ASME 1930;52:190-204.

[13] K. Washizu, Variational Methods in Elasticity and Plasticity, Pergamon Press, Oxford, 1968.

[14] M.A Martinez, F. Velasco, J.Abenojar, M. Pantoja, J.C. Del Real. Analytical solution to calculate the stress distribution in pin-and-collar samples bonded with anaerobic adhesives (following ISO 10123 standard). Int. J. Adhes. Adhes. 2008;28:405-410.

[15] L. Goglio, D. Paolino. Adhesive stresses in axially-loaded tubular bonded joints - Part II: development of an explicit closed-form solution. Int. J. Adhes. Adhes., *submitted* (*companion paper*).

[16] D.B. Bogy. Two edge-bonded elastic wedges of different materials and wedge angles under surface tractions. J. Appl. Mech. 1971;38:377-386.

[17] J.Y. Cognard, H. Devaux, L. Sohier. Numerical analysis and optimisation of cylindrical adhesive joints under tensile loads. Int. J. Adhes. Adhes. 2010;30:706-719.

[18] L. Goglio, M. Rossetto, E. Dragoni. Design of adhesive joints based on peak elastic stresses. Int. J. Adhes. Adhes. 2008;28:427-435.

[19] E. Dragoni, L. Goglio, F. Kleiner. Designing bonded joints by means of the JointCalc software. Int. J. Adhes. Adhes. 2010;30:267-280.

[20] S.M.H. Hosseini, A. Oechsner. A comparative numerical study of the stress states in flat and cylindrical lap joints. J. Adhesion Sci. Technol. 2009;23:1369-1382.

[21] L. Goglio, M. Rossetto. Precision of the one-dimensional solutions for bonded double lap joints Int. J. Adhes. Adhes. 2011;31:301-314.

TABLE CAPTIONS

Table 1. Characteristic dimensions, elastic properties and loading of the five joints used as case studies.

Table 2. Stress results from the linear and non-linear analyses of joint 1 under increasing loads.

Table 3. Comparison of linear and non-linear stresses for all joints under mean shear stresses of 1 and 50 MPa. The last row shows the corresponding values of the moment factor *k* [2] for planar lap shear joints.

FIGURE CAPTIONS

Figure 1. Infinitesimal free body diagrams for the Lubkin and Reissner [1] model: longitudinal section (to left) and cross section (to right).

Figure 2. Schematic for the model of Nayab-Hashemi *et al*. [4].

Figure 3. Schematic for the model of Pugno and Carpinteri [5].

Figure 4. Schematic for the model of Nemeş *et al*. [6].

Figure 5. Schematic drawing of the axially-loaded tubular joint with characteristic dimensions and elastic properties of the parts (adhesive thickness shown

exaggerated).

Figure 6. Outline of the geometry of joint 1 (a) with details of the overlap portion (b) and of the FE mesh (c).

Figure 7. Contour plot of normal axial stresses (σ_x) superimposed on the deformed configuration (×500) of joint 1.

Figure 8. Contour plot of shear stresses (τ_{xy}) in adherends and adhesive close to the left end of the overlap.

Figure 9. Normalized stress distributions (lines) at mid-thickness of the adhesive given by finite elements (FE) for the five joints of Table 1. The corresponding results of the Lubkin and Reissner (L&R) model (symbols) are superposed for comparison. All stresses are normalized over the mean shear stress (τ_m) given in Table 1.

Figure 10. Normalized stress distributions (lines) at mid-thickness of the adhesive given by the analytical models by Nayeb-Hashemi *et al.* [4] (N-H et al.) and by Pugno and Carpinteri [5] (P & C), for the five joints of Table 1. The corresponding results of the Lubkin and Reissner (L & R) model (symbols) are superposed for comparison. All stresses are normalized over the mean shear stress (τ_m) given in Table 1.

Figure 11. Normalized stress distributions at mid-thickness of the adhesive obtained by finite element analysis of the example 1 reported by Shi and Cheng [3].

Table 1. Characteristic dimensions, elastic properties and loading of the five joints used as case studies
(the number of significant digits for radii a_1 and a_2 is needed to give the correct value of the adhesive thickness η).

No.	a_1 (mm)	t_1 (mm)	a_2 (mm)	t_2 (mm)	a (mm)	η (mm)	$2c$ (mm)	E_1 (GPa)	ν_1 ---	E_2 (GPa)	ν_2 ---	E_a (MPa)	G_a (MPa)	β ---	F (N)	τ_m (MPa)
1	48.625	2.5	51.375	2.5	50	0.25	25.0	200	0.3	200	0.3	1000	375	20	7854	1.0
2	22.375	5.0	27.625	5.0	25	0.25	10.0	80	0.3	80	0.3	1000	375	4	1571	1.0
3	4.625	0.5	5.375	0.5	5	0.25	5.0	200	0.3	200	0.3	1000	375	100	157	1.0
4	123.625	2.5	126.375	2.5	125	0.25	12.5	200	0.3	200	0.3	1000	375	20	9818	1.0
5	4.625	0.5	5.375	0.5	5	0.25	2.5	200	0.3	200	0.3	1000	375	100	78	1.0

Table 2. Stress results from the linear and non-linear analyses of joint 1 under increasing loads.

Stress	Analysis type						
	Linear	Non-linear					
τ_m (MPa)	1	1	10	20	30	40	50
$\frac{\tau_{xy\,max}}{\tau_m}$	1.40	1.40	1.40	1.40	1.38	1.38	1.37
$\frac{\sigma_{y\,max}}{\tau_m}$	1.03	1.03	1.04	1.06	1.07	1.09	1.11
$\frac{\sigma_{z\,max}}{\tau_m}$	0.48	0.48	0.48	0.49	0.49	0.50	0.50
$\frac{\sigma_{x\,max}}{\tau_m}$	0.47	0.47	0.47	0.48	0.48	0.49	0.49

Table 3. Comparison of linear and non-linear stresses for all joints under mean shear stresses of 1 and 50 MPa. The last row shows the corresponding values of the moment factor k [2] for planar lap shear joints.

Stress	Joint No.									
	1		2		3		4		5	
τ_m (MPa)	1	50	1	50	1	50	1	50	1	50
$\frac{(\tau_{xy\,max})_{Nonlinear}}{(\tau_{xy\,max})_{Linear}}$	0.999	0.974	0.999	0.958	1.000	0.978	0.999	0.968	1.000	0.972
$\frac{(\sigma_{y\,max})_{Nonlinear}}{(\sigma_{y\,max})_{Linear}}$	1.001	1.077	1.001	1.074	1.007	1.282	1.000	1.018	1.007	1.262
$\frac{(\sigma_{z\,max})_{Nonlinear}}{(\sigma_{z\,max})_{Linear}}$	1.002	1.052	1.000	1.055	1.005	1.209	1.002	1.010	1.000	1.195
$\frac{(\sigma_{x\,max})_{Nonlinear}}{(\sigma_{x\,max})_{Linear}}$	1.002	1.056	1.000	1.053	1.006	1.228	1.002	1.013	1.007	1.261
k	0.90	0.56	0.98	0.90	0.92	0.62	0.96	0.78	0.97	0.82

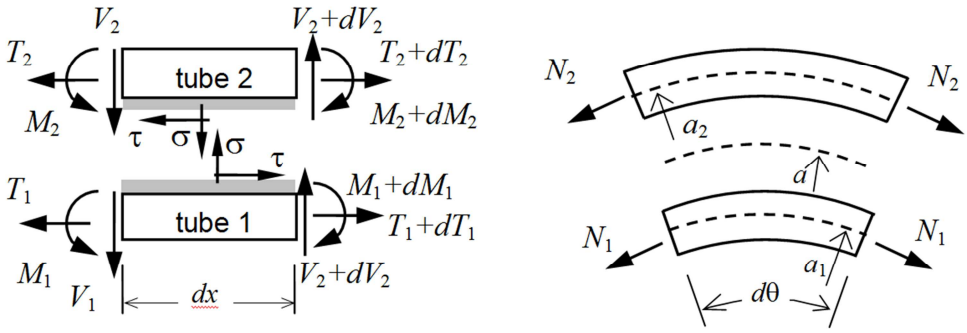

Figure 1. Infinitesimal free body diagrams for the Lubkin and Reissner [1] model: longitudinal section (to left) and cross section (to right).

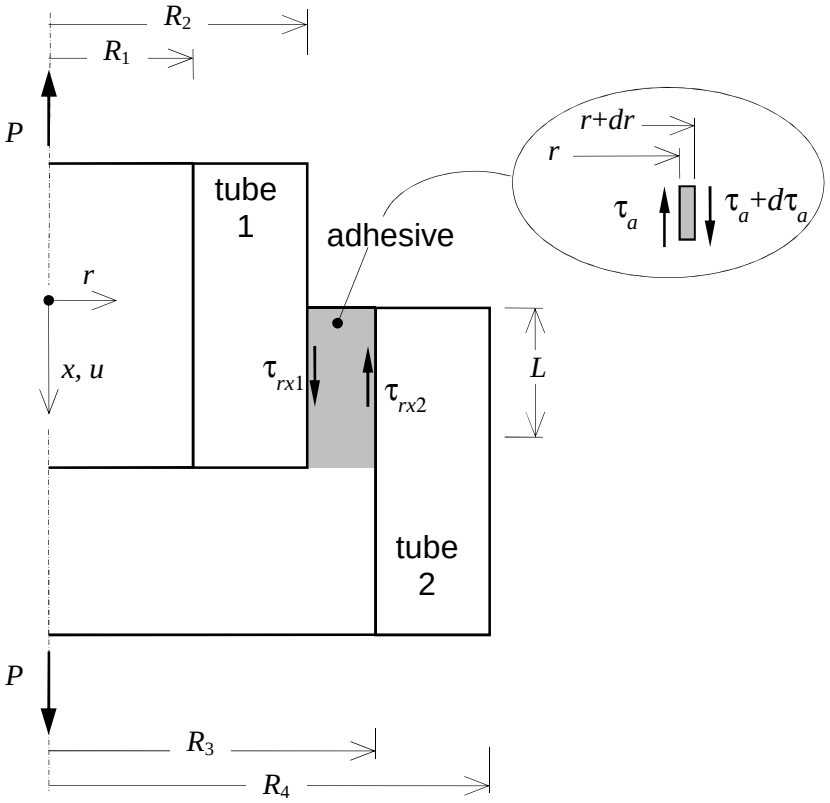

Figure 2. Schematic for the model of Nayab-Hashemi *et al*. [4].

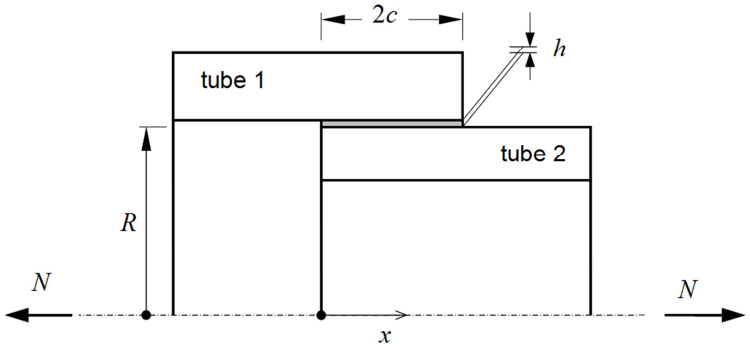

Figure 3. Schematic for the model of Pugno and Carpinteri [5].

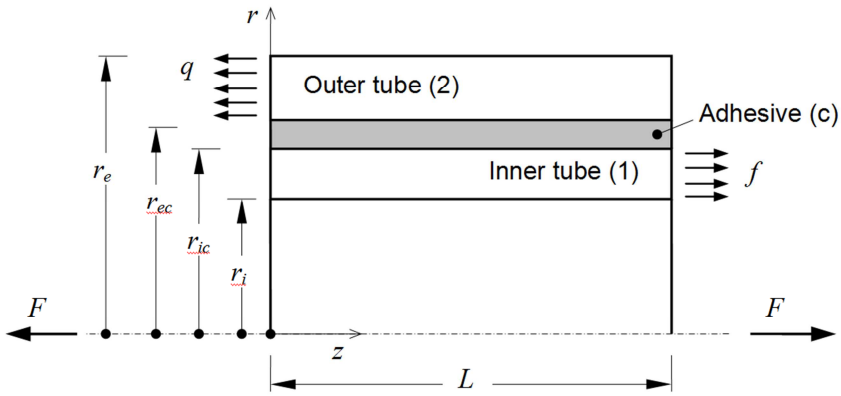

Figure 4. Schematic for the model of Nemeş *et al.* [6].

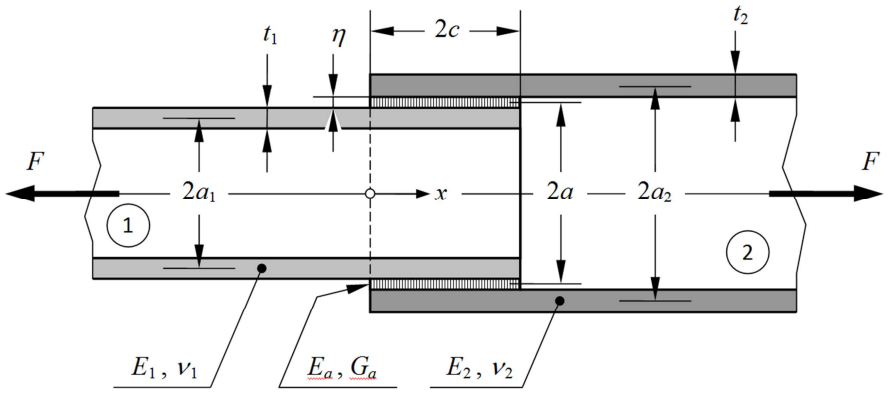

Figure 5. Schematic drawing of the axially-loaded tubular joint with characteristic dimensions and elastic properties of the parts (adhesive thickness shown exaggerated).

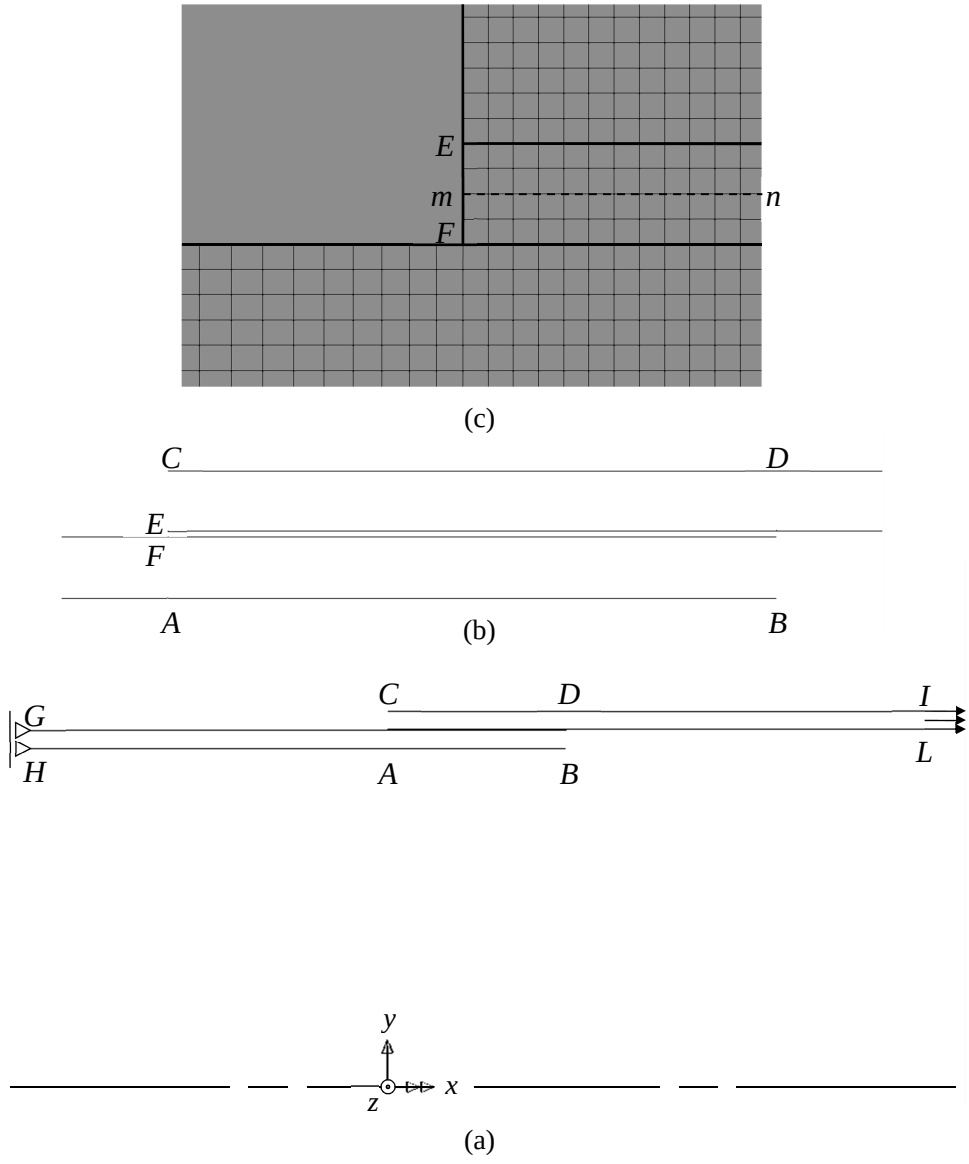

Figure 6. Outline of the geometry of joint 1 (a) with details of the overlap portion (b) and of the FE mesh (c).

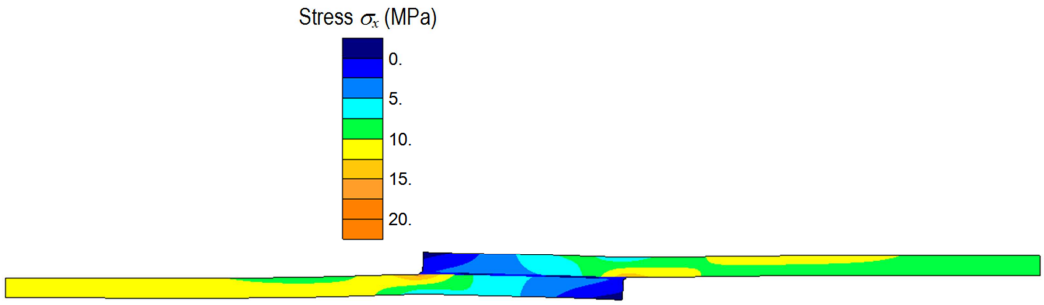

Figure 7. Contour plot of normal axial stresses (σ_x) superimposed on the deformed configuration (×500) of joint 1.

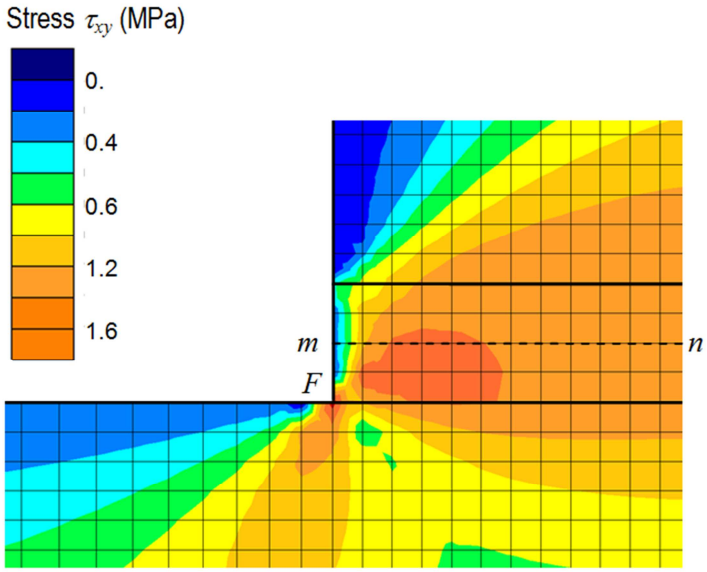

Figure 8. Contour plot of shear stresses (τ_{xy}) in adherends and adhesive close to the left end of the overlap.

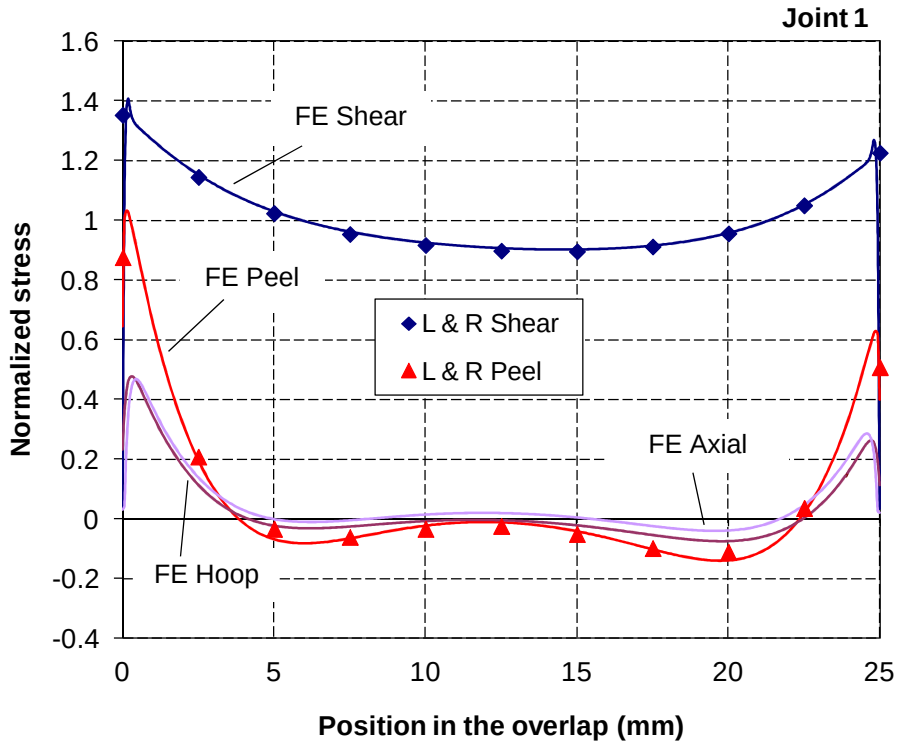
Joint 1
Normalized stress
1.6
1.4
1.2
1
0.8
0.6
0.4
0.2
0
-0.2
-0.4
0
5
10
15
20
25
Position in the overlap (mm)
FE Shear
FE Peel
L & R Shear
L & R Peel
FE Axial
FE Hoop

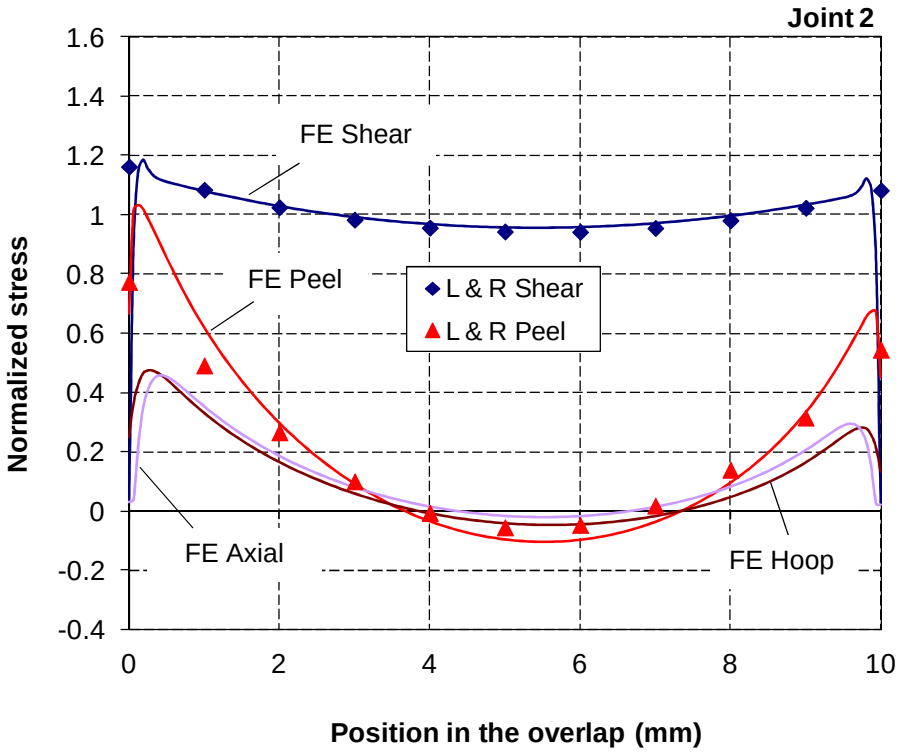
Joint 2
Normalized stress
1.6
1.4
1.2
1
0.8
0.6
0.4
0.2
0
-0.2
-0.4
0
2
4
6
8
10
Position in the overlap (mm)
FE Shear
FE Peel
L & R Shear
L & R Peel
FE Axial
FE Hoop

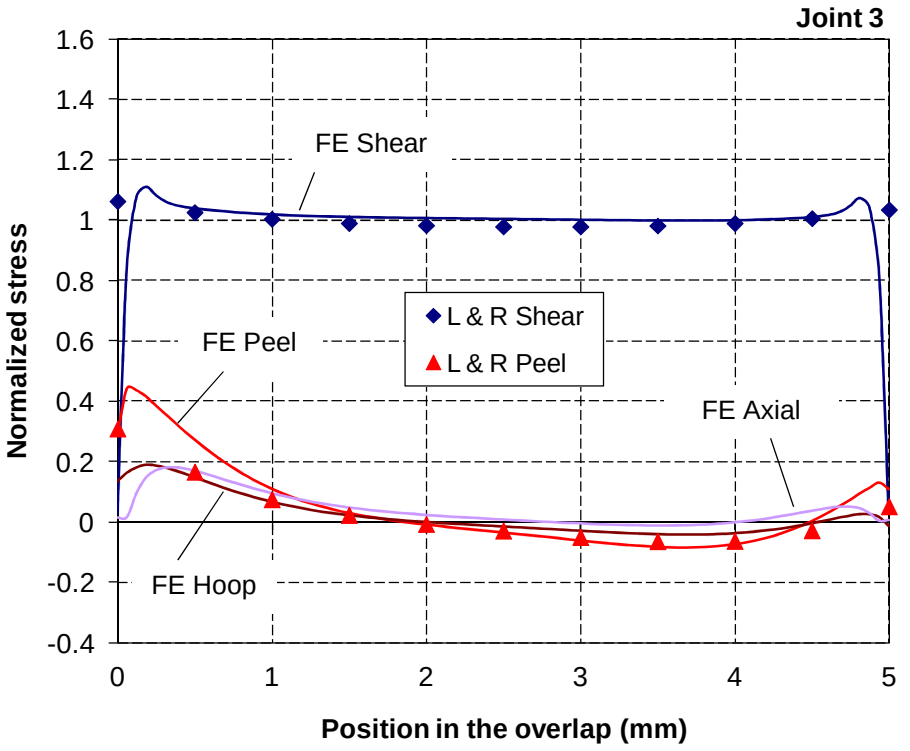
Joint 3
1.6
1.4
1.2
1
0.8
0.6
0.4
0.2
0
-0.2
-0.4
Normalized stress
FE Shear
FE Peel
FE Hoop
FE Axial
L & R Shear
L & R Peel
0
1
2
3
4
5
Position in the overlap (mm)

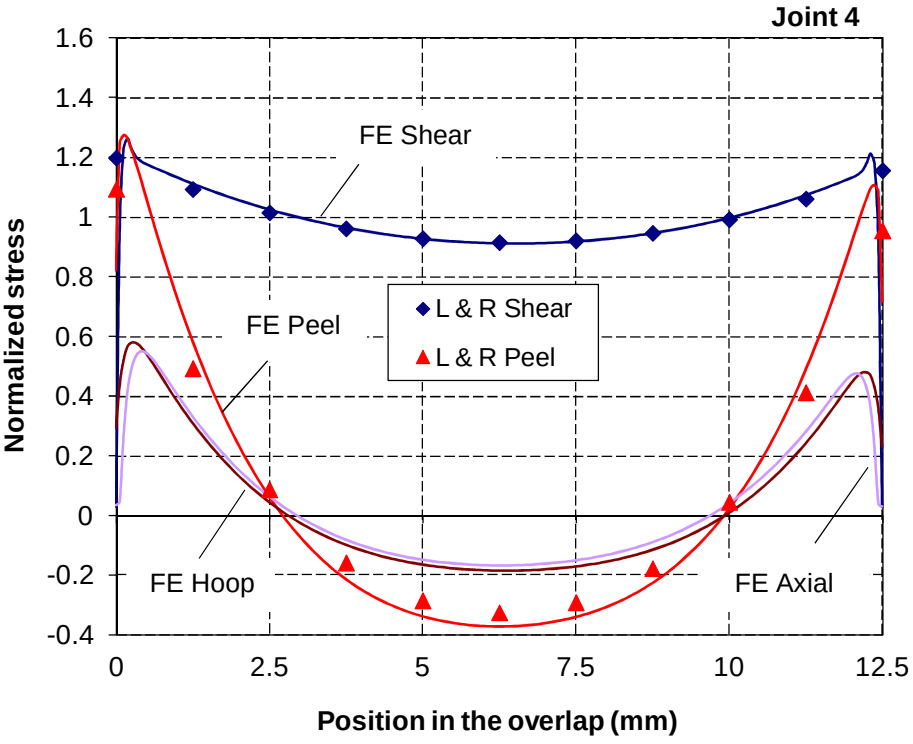
Joint 4
1.6
1.4
1.2
1
0.8
0.6
0.4
0.2
0
-0.2
-0.4
Normalized stress
FE Shear
FE Peel
FE Hoop
FE Axial
L & R Shear
L & R Peel
0
2.5
5
7.5
10
12.5
Position in the overlap (mm)

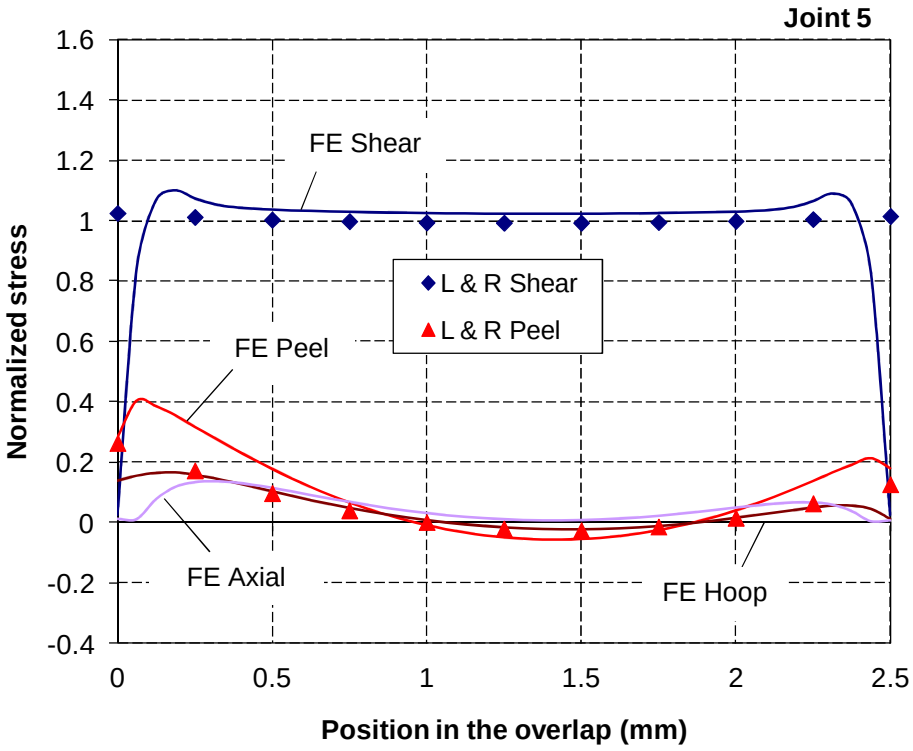

Figure 9. Normalized stress distributions (lines) at mid-thickness of the adhesive given by finite elements (FE) for the five joints of Table 1. The corresponding results of the Lubkin and Reissner (L & R) model (symbols) are superposed for comparison. All stresses are normalized over the mean shear stress (τ_m) given in Table 1.

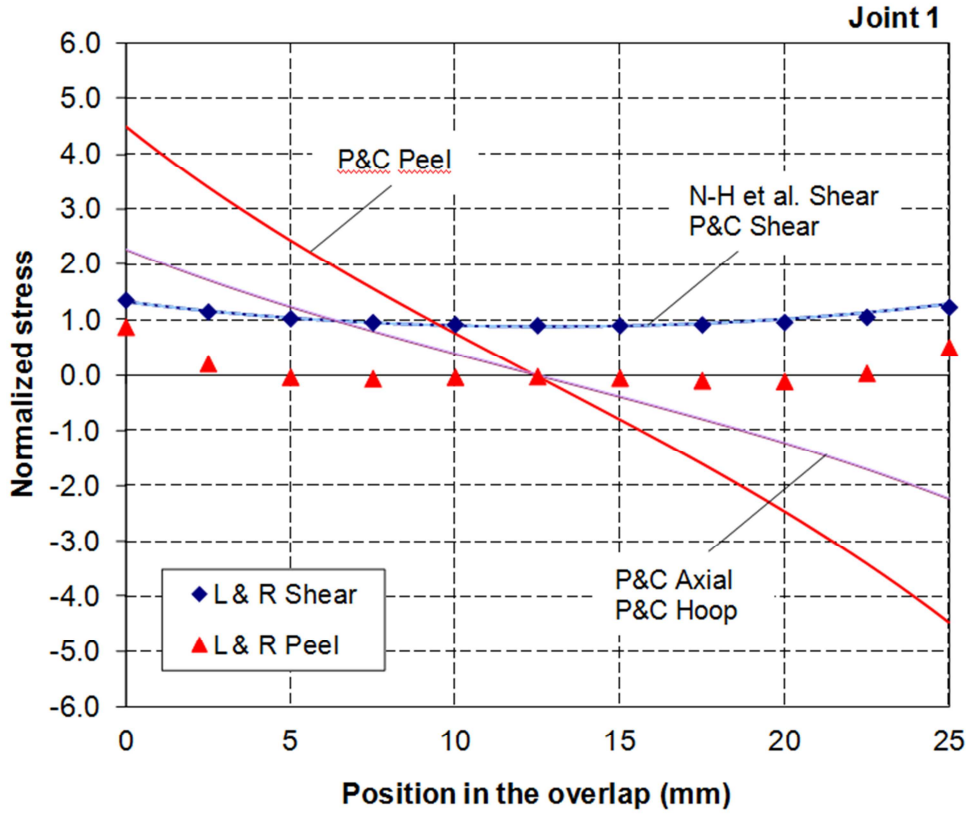
Joint 1
6.0
5.0
4.0
3.0
2.0
1.0
0.0
-1.0
-2.0
-3.0
-4.0
-5.0
-6.0
Normalized stress
P&C Peel
N-H et al. Shear
P&C Shear
P&C Axial
P&C Hoop
L & R Shear
L & R Peel
0
5
10
15
20
25
Position in the overlap (mm)

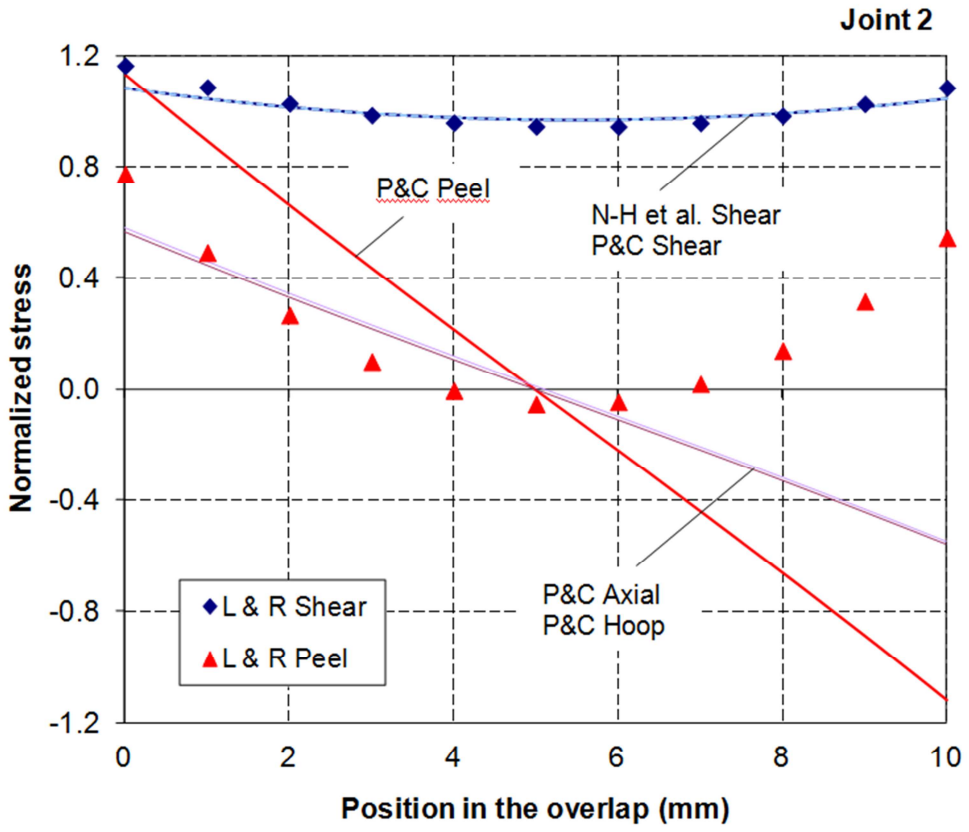
Joint 2
1.2
0.8
0.4
0.0
-0.4
-0.8
-1.2
Normalized stress
P&C Peel
N-H et al. Shear
P&C Shear
P&C Axial
P&C Hoop
L & R Shear
L & R Peel
0
2
4
6
8
10
Position in the overlap (mm)

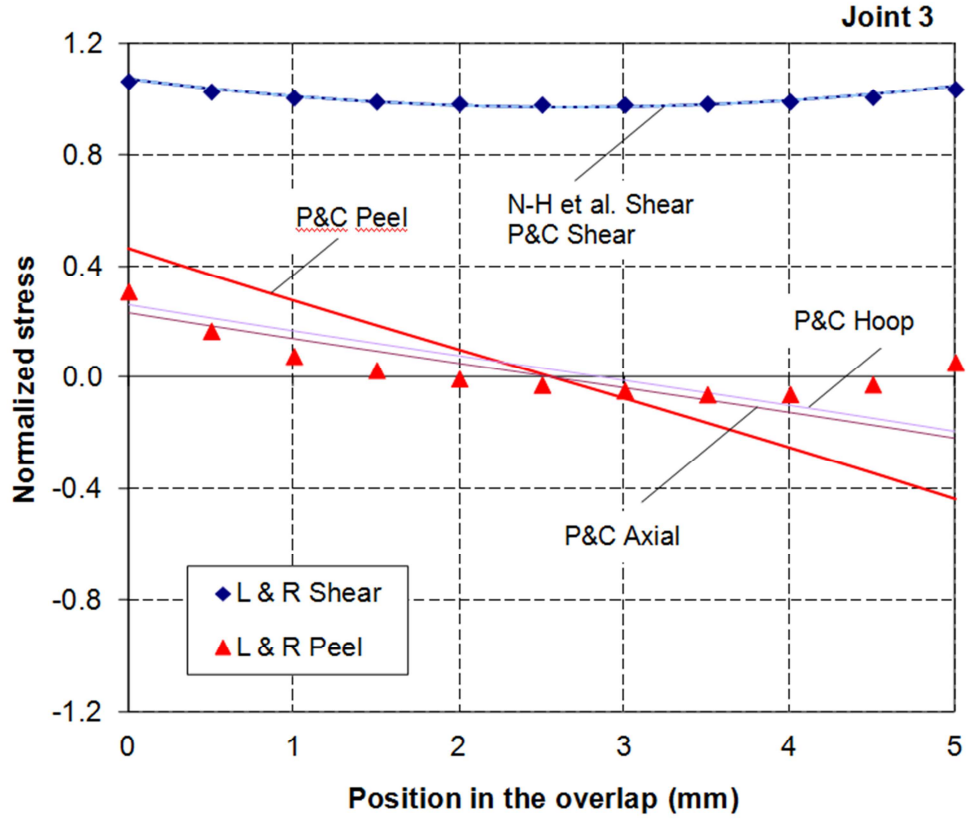
Joint 3
1.2
0.8
0.4
0.0
-0.4
-0.8
-1.2
Normalized stress
0
1
2
3
4
5
Position in the overlap (mm)
P&C Peel
N-H et al. Shear
P&C Shear
P&C Hoop
P&C Axial
L & R Shear
L & R Peel

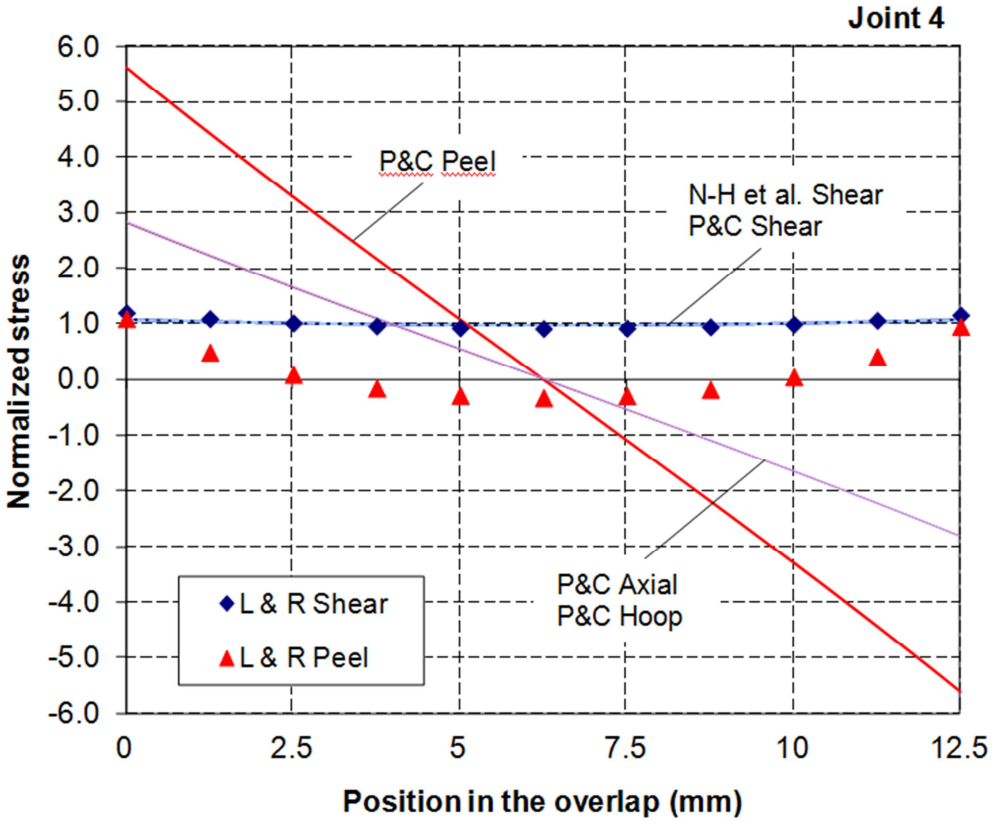
Joint 4
6.0
5.0
4.0
3.0
2.0
1.0
0.0
-1.0
-2.0
-3.0
-4.0
-5.0
-6.0
Normalized stress
0
2.5
5
7.5
10
12.5
Position in the overlap (mm)
P&C Peel
N-H et al. Shear
P&C Shear
P&C Axial
P&C Hoop
L & R Shear
L & R Peel

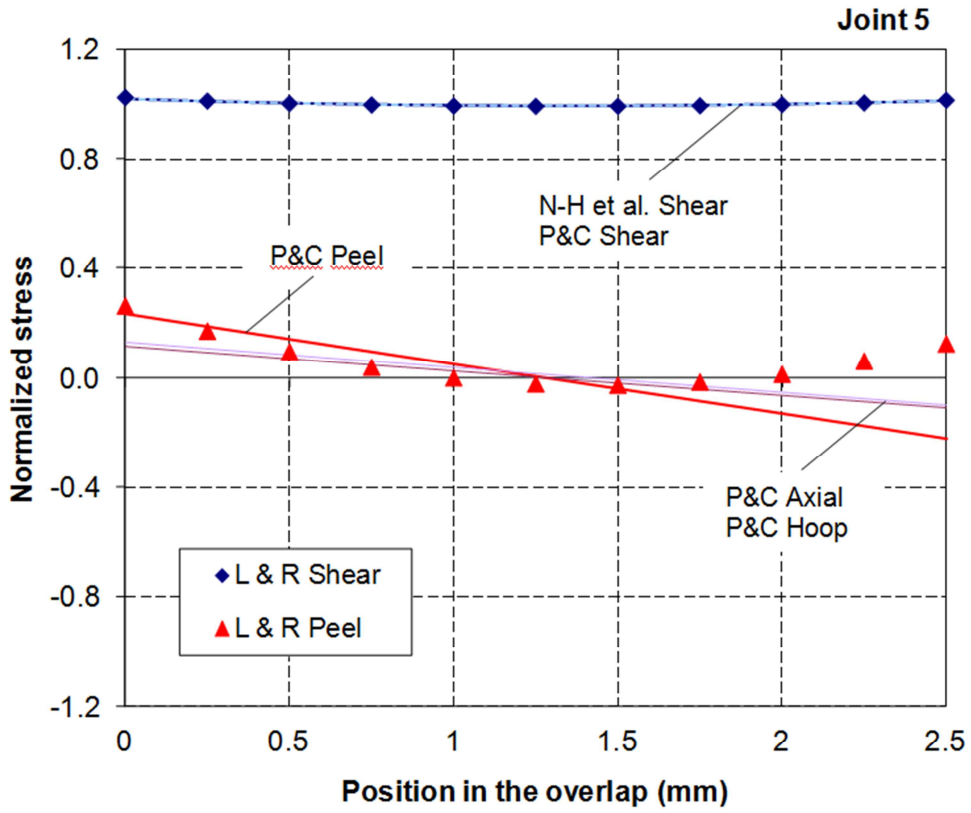

Figure 10. Normalized stress distributions (lines) at mid-thickness of the adhesive given by the analytical models by Nayeb-Hashemi *et al.* [4] (N-H et al.) and by Pugno and Carpinteri [5] (P & C), for the five joints of Table 1. The corresponding results of the Lubkin and Reissner (L & R) model (symbols) are superposed for comparison. All stresses are normalized over the mean shear stress (τ_m) given in Table 1.

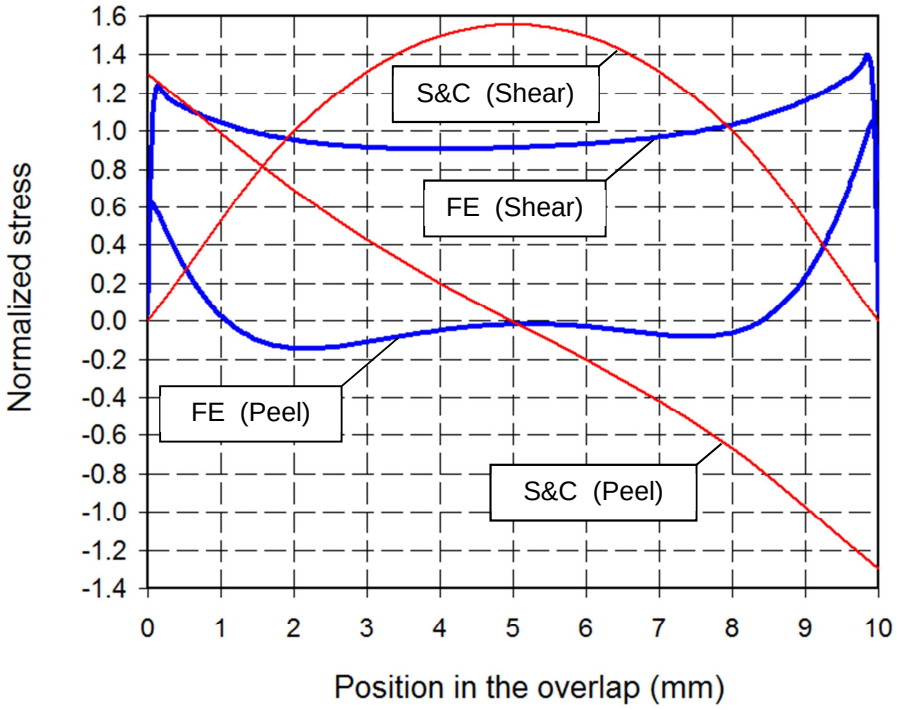

Figure 11. Normalized stress distributions at mid-thickness of the adhesive obtained by finite element analysis (FE) of the example 1 reported by Shi and Cheng (S&C) [3].